DOI: 10.3969/j.issn.1673-3185.2017.02.016 **http:** // english.ship-research.com

Translated from: ZHANG W K, WANG G X, XU G H, et al. Development of control system in abdominal operating ROV[J]. Chinese Journal of Ship Research, 2017, 12(2): 124-132.

Development of control system in abdominal operating ROV

ZHANG Weikang[1], *WANG Guanxue*[1], *XU Guohua*[1], *LIU Chang*[1], *SHEN Xiong*[2]

1 School of Naval Architecture and Ocean Engineering, Huazhong University of Science and Technology, Wuhan 430074, China

2 Wuhan Second Ship Design and Research Institute, Wuhan 430205, China

Abstract: In order to satisfy all the recovery requirements of Unmanned Underwater Vehicle (UUV), a new type of abdominal operating Remote Operated Vehicle (ROV) was developed. The abdominal operating ROV is different from the general ROV which works by a manipulator, and it completes the docking and recovery tasks of UUVs with its abdominal operating mechanism. In this paper, the system composition and principles of the abdominal operating ROV are presented. We then propose a framework for a control system in which the integrated industrial reinforced computer acts as a surface monitor unit, while the PC104 embedded industrial computer acts as the underwater main control unit and the other driver boards act as the driver unit. In addition, the dynamics model and a *H*-infinity robust controller for automatic orientation in the horizontal plane were designed and built. Individual tests, system joint test and underwater tests show that this control system has good real-time performance and reliability, and it can complete the recovery task of a UUV. The presented structure and algorithm could provide reference for the control system development of mobile robots, drones and biomimetic robot.

Key words: abdominal operating ROV; control system; PC104; *H*-infinity robust control

CLC number: U674.941

0 Introduction

With the development of the world economy, science and technology, mankind has accelerated the pace of development of marine resources. In order to improve the development of marine resources, resolutely safeguard the national maritime rights and interests, and build China into a maritime power, the development of national marine technology is urgent, especially in the deep-sea exploration, transportation and operation technology[1].

Underwater vehicle is one of the important tools for the exploration and development of marine resources. According to whether it is manned or not, it can be divided into Unmanned Underwater Vehicle (UUV) and Human Occupied Vehicle (HOV). Moreover, UUV can be divided into Remotely Operated Vehicle (ROV) and Autonomous Underwater Vehicle (AUV) according to its control mode[2]. In recent years, UUV has been widely used in marine exploration, development, search, rescue and other fields, and a typical case is that the "bluefin tuna" was used in the search of the wreckage of Malaysia airplane[3].

Although UUV technology has made great progress in the last century, the recovery of UUV has become a problem that must be solved for the complicated environment of underwater and the limited power of cableless UUV with the complexity of control[4-6]. At present, the main operating means of abdominal operation underwater vehicle used for the docking and recovery of UUV in China and abroad are multi-manipulator collaborative grasping or hydraulic U-shaped clamping, which are difficult to control, easy to cause marine pollution and have large volume, etc.[7-8]. In this paper, the abdominal operating Remotely Operated Vehicle (called abdomi-

Received: 2016-07-08

Author(s): ZHANG Weikang, male, born in 1992, master candidate. Research interest: control strategy for underwater vehicle. E-mail: zhangweikanghust@163.com

XU Guohua (Corresponding author), male, born in 1965, Ph.D., professor, doctoral supervisor. Research interests: underwater vehicle and intelligent control methods. E-mail: hustxu@vip.sina.com

nal operating ROV for short) uses the electric-driven abdominal operating mechanism with guide cylinder to guide and lock the docking pole of UUV which finally completes the capturing and recovery. Such new abdominal operating ROV has advantages like small size, low pollution and low power consumption. The reliability of the control system is the prerequisite and guarantee for the completion of the assigned task by abdominal operating ROV.

1 System configuration of the abdominal operating ROV

Abdominal operating ROV system is generally divided into three components: water-surface monitoring station, umbilical cable and ROV body. The general technical specification of system is shown in Table 1, and the system structure is shown in Fig. 1. Moreover, the devices layout of ROV body is shown in Fig. 2.

Table 1 The general technical specification

Index	Content
Size/mm	700×550×425
Weight (in air)/kg	53.8
Working depth/m	300
Power supply	DC voltage-stabilized source
Umbilical cable	Diameter of 20 mm and breaking force of 441 kN
Propeller	2 main propellers, 1 side propeller, 2 vertical propellers
Operating device	1 electric-driven push rod
Navigation device	1 attitude instrument (integrated magnetic compass, depthometer, inclinometer)
Equipment for observation and communication	2 halogen lamps, 1 color camera with PTZ

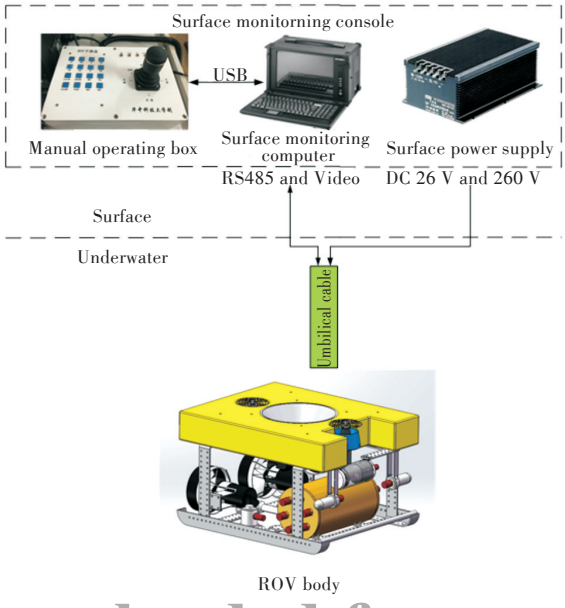

Fig.1 The system structure of abdominal operating ROV

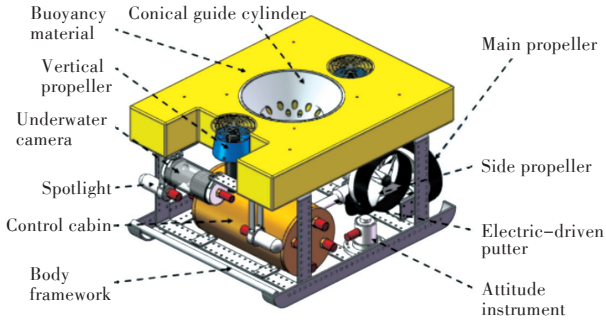

Fig.2 The devices layout of abdominal operating ROV

During the capture and recovery operation of abdominal operating ROV, the operator first operates the manual box according to the video information of the underwater camera displayed by the surface monitoring computer and sends the information to the underwater controller via surface monitoring software so as to drive the ROV body, thus searching for and approaching to the UUV; when ROV is close to the UUV, the docking pole stretching out from UUV bottom is searched by rotating the camera; ROV is used to make the docking pole insert into the conical guide cylinder of abdominal operating mechanism at the center of the ROV buoyancy material, and meanwhile, the electric-driven push rod of abdominal operating mechanism (located in the center line of ROV stern) is stretched into the locking hole of UUV docking pole, thus finishing the capture and docking tasks of UUV. The docking process is shown in Fig. 3-Fig. 4.

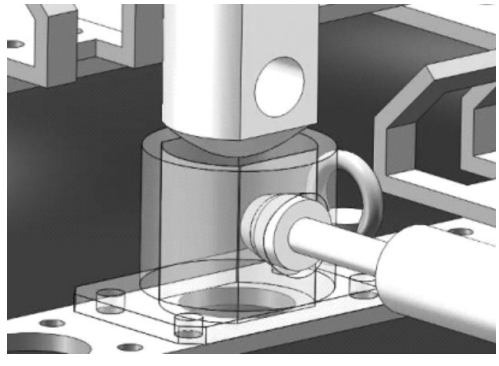

Fig.3 During the docking task

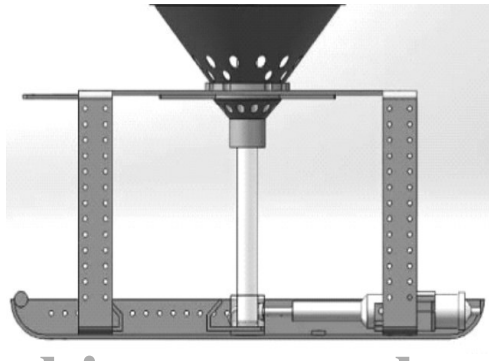

Fig.4 Complete the docking task

2 Structure of control system

The control system structure of the abdominal operating ROV is shown in Fig. 5, which is mainly divided into two components: surface control console and underwater controller, and the data communication and transmission of video signal and power of both are directly through the zero-buoyancy umbilical cable.

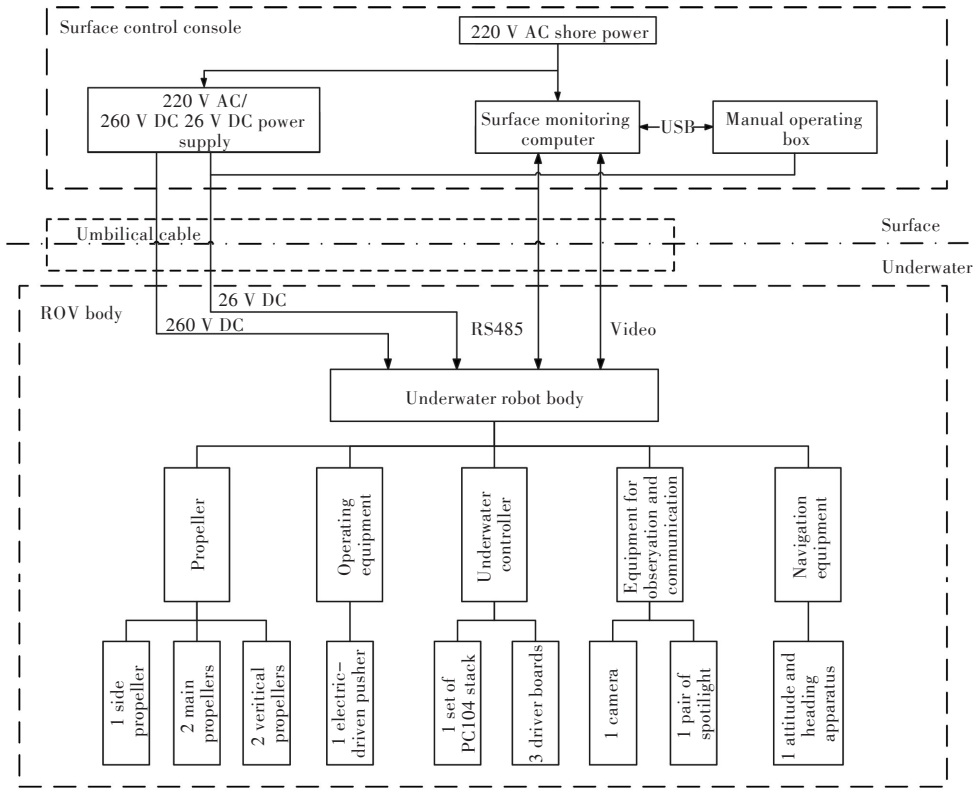

Fig.5 The control system structure of the abdominal operating ROV

2.1 Surface control console

Surface control console is constituted of manual operating box, surface monitoring computer, surface DC voltage-stabilized source, and the block diagram of the composition is shown in Fig. 6.

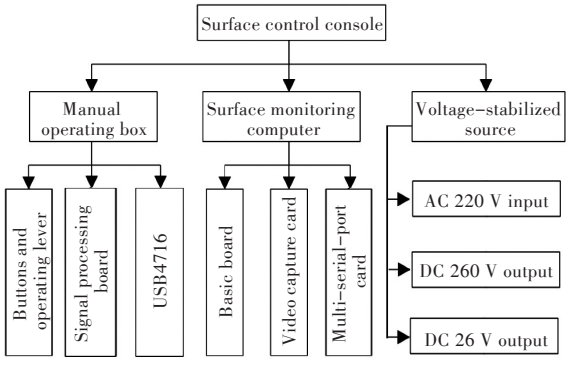

Fig.6 The constitution diagram of surface control console

The manual operating box consists of three-axis control lever, button, signal-processing board and USB4716 acquisition module. The signal processing board converts the input DC 26 V power supply to DC 5 V, then supplies power to the operating level and button and converts it into the analogue and digital signals within the input range of USB4716 capture card; the USB4716 sends the collected signal to the surface monitoring computer through the USB bus. The surface monitoring computer is an integrated industrial reinforced computer from Advantech company, which is mainly composed of basic board, video capture card and multi-serial-port card, and the video capture card collects the video signal sent back from the underwater camera, while the multi-serial-port card provides the RS485 serial port so as to communicate with the main underwater controller.

To provide a friendly visualization of man-machine interface, the surface monitoring software is developed based on VC++ 6.0 and operated in the Windows XP operating system with the operating interface shown in Fig. 7, and the block diagram of surface monitoring software is shown in Fig. 8.

The left side of the interface of surface monitoring software is the real-time video image sent by the abdominal ROV camera, while the right side is the current ROV working state, such as the communicating

Fig.7 The running interface of surface monitor software

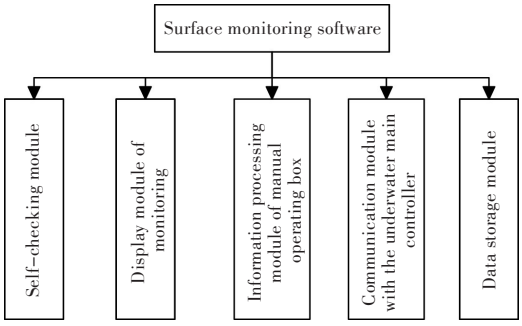

Fig.8 The constitution diagram of surface software

status with the manual operating box, underwater main controller, main driver board (PWM board 1), and side driver board (PWM board 2), the detecting status of the control cabin leakage of the underwater main controller and the current depth, course, pitch and heel of ROV. The layout of surface monitoring software is simple and clear with satisfying operability.

The Chaoyang QT30 customized supply is selected as the surface voltage-stabilized source. In order to ensure the reliable isolation of the power supply and the control supply, the two-way output is applied. After the calculation of load power, the power supply output is selected as DC 260 V/3 000 W, while the control supply is DC 26 V/100 W. The output of power supply is as the main supply for the underwater propeller, electric-driven push rod, spotlight and other equipment, while the output of control supply is as the supply for the circuit boards of underwater controller, underwater cameras and PTZ.

2.2 Underwater controller

The underwater controller is installed in a control cabin with an appearance structure of cylindrical, waterproof and pressure-resistant shell (see in Fig. 9). The overall shape of the control cabin is cylindrical with length of 350 mm, diameter of 198 mm, thickness of 9 mm and displacement of 10.77 kg. The end caps with O-shaped seal ring are at its both ends and the waterproof connector is installed on the outer surface of the end cap, then the connection between the underwater controller and the external device is established. The diagram of underwater controller hardware is shown in Fig. 10[9].

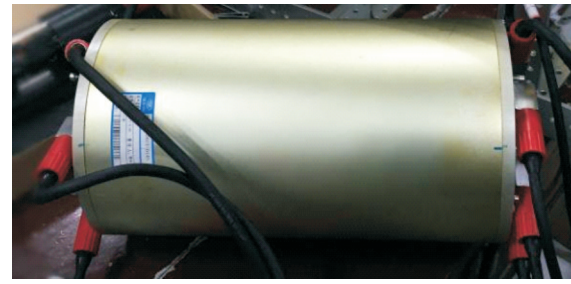

Fig.9 The compressive cabin

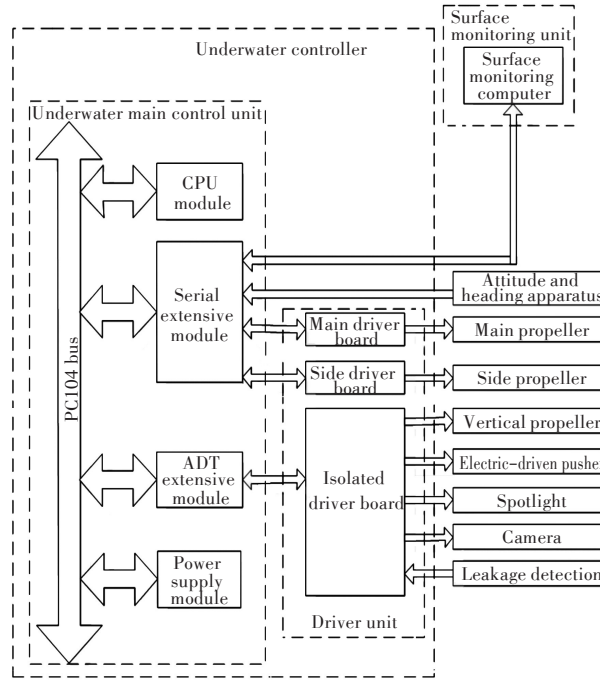

Fig.10 The diagram of underwater controller hardware

The underwater master unit is a PC104 embedded industrial control computer, which consists of 4 stack modules through PC104 bus interconnection. The underwater master control unit is the control center of the control system, and its software module is shown in Fig. 11. The underwater master control unit is responsible for receiving the instructions sent by the monitoring computer. After the integrated processing and calculation, it is distributed to the driver boards in a certain time-sequence, and the state information from the attitude and heading apparatus and the feedback of the driver board plates are collected and processed, which are sent to the surface monitoring computer.

The driving unit is composed of the main driver board, the side driver board and the isolated driver board. The driving unit serves as the bridge between

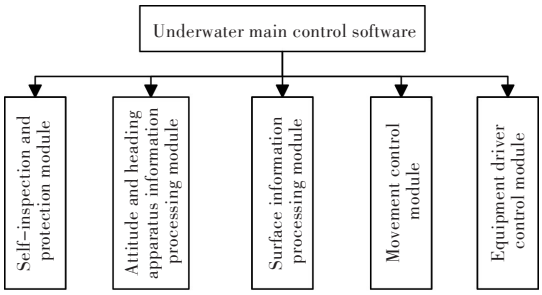

Fig.11 The diagram of underwater master controller software

the underwater main-control unit and the external actuator, whose main function is to ensure the electrical isolation between the underwater main-control unit and the actuator, and to reduce the electromagnetic interference of actuator on underwater main-control unit.

3 Dynamics modeling

3.1 Six Degree of Freedom (DoF) space motion equation

Considering the general situation that the center of gravity G of the underwater vehicle does not coincide with the origin O of the carrier coordinate system, the general form of the 6-DoF motion equation of the underwater vehicle can be obtained according to the relationship between the translational motion and the rotational motion of the rigid body [10]:

$$X = m[\dot{u} - vr + wq - x_G(q^2 + r^2) + y_G(pq - \dot{r}) + z_G(pr + \dot{q})] \quad (1)$$

$$Y = m[\dot{v} - wp + ur - y_G(r^2 + p^2) + z_G(qr - \dot{p}) + x_G(qp + \dot{r})] \quad (2)$$

$$Z = m[\dot{w} - uq + vp - z_G(p^2 + q^2) + x_G(rp - \dot{q}) + y_G(rq + \dot{p})] \quad (3)$$

$$K = m[y_G(\dot{w} - uq + vp) - z_G(\dot{v} - wp + ur)] + I_x\dot{p} + (I_z - I_y)qr \quad (4)$$

$$M = m[z_G(\dot{u} + wq - vr) - x_G(\dot{w} + vp - uq)] + I_y\dot{q} + (I_x - I_z)rp \quad (5)$$

$$N = m[x_G(\dot{v} + ur - wp) - y_G(\dot{u} + wp - vr)] + I_z\dot{r} + (I_y - I_x)pq \quad (6)$$

where m is the mass of the underwater vehicle; x_G, y_G and z_G are the coordinates of the center of gravity of the underwater vehicle in the carrier coordinate system; I_x, I_y and I_z are the rotational inertia of the underwater vehicle to x, y and z axes; N is the resultant moment when the ROV turns; r is the steering angular velocity; the specific meaning of the remaining variables can be found in the Reference [10].

For ROV, its motion control is generally in remote control mode, and supplemented by automatic depth setting and automatic orientation. Therefore, for the abdominal operating ROV in this paper, the horizontal-plane dynamic equation and vertical-plane dynamic equation can be separated, and then the modeling and controller design for the automatic control of orientation and depth can be completed. Due to space limitations, only the horizontal-plane dynamic equation and automatic orientation control are studied in this paper.

3.2 Horizontal-plane dynamic equation

For the abdominal operating ROV, the buoyancy material is located in the upper part of the robot body, which can approach to the state of zero buoyancy when working under water by adjusting the counterweight. By the 3D modeling software SolidWorks2012, it can be calculated that the center of buoyancy and the center of gravity are basically in a vertical line, and the center of buoyancy is 105.280 mm higher than that of the gravity, which can guarantee a large restoring moment. Therefore, there is strong self-stability on the pitch and heel DOF, and in the analysis of the horizontal-plane motion equation, the motion coupling between the planes perpendicular to each other can be ignored for simplicity. The horizontal-plane motion equation can be separated as

$$X = m(\dot{u} - vr - x_G r^2 - y_G\dot{r}) \quad (7)$$

$$Y = m(\dot{v} + ur - y_G r^2 - x_G\dot{r}) \quad (8)$$

$$N = I_z\dot{r} + m[x_G(\dot{v} + ur) - y_G(\dot{u} - vr)] \quad (9)$$

In this paper, the origin of the carrier coordinate system coincides with the center of gravity of the underwater vehicle, that is, $x_G = y_G = z_G = 0$, and then the horizontal-plane motion equation is further simplified as

$$X = m(\dot{u} - vr) \quad (10)$$

$$Y = m(\dot{v} + ur) \quad (11)$$

$$N = I_z\dot{r} \quad (12)$$

3.3 Transfer function of orientation control

For the orientation control of ROV, the diagram is shown in Fig. 12[11], where ψ_{ref} is the given course angle; e is the deviation of course angle; n is the rotating speed of propeller; T_{pro} is the moment of thrust generated by the propeller; ψ is the course angle of ROV.

Firstly Eq. (12) is analyzed. For underwater vehicle, the resultant moment when it rotates is

$$N = T_{\text{pro}} - F_N - R_N \quad (13)$$

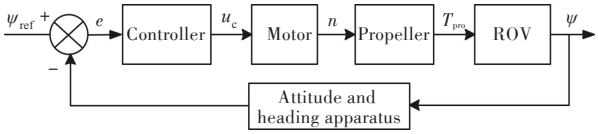

Fig.12 The diagram of automatic orientation

where F_N is the inertia moment generated by the additional rotational inertia; R_N is the resisting moment generated by the resistance. From Reference [11−12], it can be inferred that:

$$F_N = N_{\dot{r}}\dot{r} \tag{14}$$

$$R_N = N_r \rho S r^2/2 \tag{15}$$

where $N_{\dot{r}}$ is the additional mass; N_r is the resistance coefficient of the fore−turning of underwater vehicle; ρ is the water density; S is the equivalent area.

Combining Eq. (13)−Eq. (15), it can be obtained that

$$T_{\text{pro}} - N_r \rho S r^2/2 = (I_z + N_{\dot{r}})\dot{r} \tag{16}$$

Considering that the angular velocity of the abdominal operating ROV is low during the automatic orientation, it is possible to conduct Taylor expansion for r^2 when $r=0$, and the Eq. (16) can be simplified as

$$\frac{T_{\text{pro}}}{I_z + N_{\dot{r}}} = \dot{r} = \ddot{\psi} \tag{17}$$

Eq. (17) represents the direct relationship between the ROV course angle and the thrust moment of the propeller, and the following transfer function can be obtained after conducted Laplace transform for it:

$$G_1(s) = \frac{\psi(s)}{T_{\text{pro}}(s)} = \frac{1}{s^2(I_z + N_{\dot{r}})} \tag{18}$$

As the propeller using brushless DC motor, its dynamic characteristics can be simplified as an inertia link, then the transfer function can be obtained after the control signal u_c is normalized:

$$G_2(s) = \frac{n(s)}{u_c(s)} = \frac{K_m}{1 + Ts} \tag{19}$$

where T is the time constant of motor; K_m is the amplification coefficient of motor.

The higher the accuracy of the propeller model is, the more conducive to the upgrade of the final control accuracy is. However, the cost of precision modeling is relatively high. In general applications of low−speed underwater vehicle, the propeller model is generally assumed as linear with symmetrically equal thrust force of the advancement and recession. In the orientation control strategy in this paper, the setting velocities of 2 main propellers are always the same but with opposite directions, thus forming a pair of couple to provide steering moment. Hence, the linearized equation of the thrust moment generated by the propeller and its rotating speed can be obtained

$$T_{\text{pro}} = Cn \tag{20}$$

where C is the coefficient of thrust moment of the propeller. Therefore, the transfer function of propeller is as

$$G_3(s) = C \tag{21}$$

Combining Eq. (18)−Eq. (21), the open−loop transfer function of the controlled object is

$$G_k(s) = G_1(s)G_2(s)G_3(s) = \frac{K_m C}{(I_z + N_{\dot{r}})(1 + Ts)s^2} \tag{22}$$

For hydrodynamic coefficients, the other similar open−frame underwater vehicle is used for reference: $N_{\dot{r}} = 0.3I_z$, $N_r = 0.2$ [12]. For I_z, by the mass attribute of 3D modeling software SolidWorks2012, it can be obtained that I_z = 3.05 kg·m^2. For the motor constant of propeller, as its rated rotating speed is 2 000 r/min, that is, 33.33 s^{-1}, K_m = 33.33 can be selected based on the definition of amplification coefficient; for T, it can be obtained that T is about 1.16 through the measurement and estimation and can be taken as T = 1.2 without loss of generality. For the coefficient C, taking the consideration that the thrust of the propeller under rated rotating speed is 25 kgf (245.2 N), and the distance between the central−axis lines of the two main propellers is 0.296 m, so the coefficient C = 25 × 9.8 × 0.296/33.33 = 2.176.

After substituting the related coefficients, there is

$$G_k(s) = \frac{18.292}{(1.2s + 1)s^2} \tag{23}$$

4 Design of orientation controller

4.1 Selection of control algorithm

There are various methods of automatic orientation control for ROV, usually PID control, fuzzy control and sliding mode variable structure control, and each method has its own advantages and disadvantages. For the abdominal operating ROV studied in this paper, due to the existence of abdominal operating mechanism, its overall appearance is different from the general open−frame ROV. Constrained by the testing funds and conditions, the accurate hydrodynamic coefficients of abdominal operating ROV are hard to obtain, so there are certain perturbations between coefficients of open−loop transfer function of orientation control obtained in Section 3.3 and the real values. To guarantee the robustness of the automatic orientation controller, an H−infinite robust controller based on hybrid sensitivity which is insensitive to

parameter perturbation is selected as the automatic orientation controller in this paper.

4.2 Design of *H*−infinite robust controller

Firstly, the block diagram of automatic orientation control in Fig. 12 is converted into a diagram about *H*−infinite control based on hybrid sensitivity as shown in Fig. 13, where $K(s)$ is the orientation controller; $G_k(s)$ is the transfer function of object; $W_1(s)$, $W_2(s)$ and $W_3(s)$ are the weighting functions; r_{ref} is the reference input (that is the given course angle); y denotes the output of measurement (that is the course angle measured by attitude and heading apparatus); z_1, z_2 and z_3 are the evaluation output after weighting.

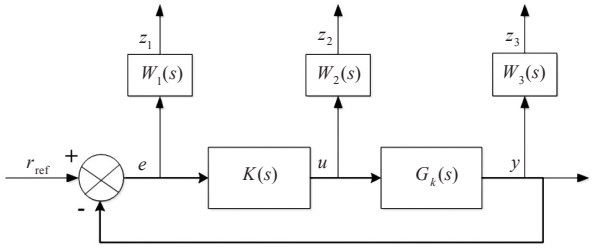

Fig.13 The diagram of mixed sensitivity H_∞ control

The core of *H*−infinite control based on hybrid sensitivity is to solve the controller $K(s)$, and to minimize the *H*−infinite norm shown in Eq. (24) or below a certain value γ under the stabilized closed−loop system.

$$\left\| \begin{matrix} W_1(I+GK)^{-1} \\ W_2K(I+GK)^{-1} \\ W_3GK(I+GK)^{-1} \end{matrix} \right\|_\infty < \gamma \tag{24}$$

The selection of $W_1(s)$ is determined by the requirements of system performance. For underwater vehicle, its reference input signal and external interference are usually low frequencies. To ensure that the system tracks the reference input signal more precisely, $W_1(s)$ should be provided with the characteristics of high−gain and low−pass. $W_2(s)$ is usually selected as a constant for limiting the controller output. There is an upper limit on the speed of the main propeller of actuator in the ROV, and the controller output u_c has been normalized during the modeling of Section 3.3, that is $u_c \in [-1, 1]$. Therefore, when $W_2(s)$ is selected, the controller output must satisfy the limitation $-1 \leqslant u_c \leqslant 1$. The selection of $W_3(s)$ should be determined by the measurement noise of sensor and the high−frequency unmodeled dynamic characteristics of system. In order to suppress the influence of measurement noise on system performance, $W_3(s)$ should have high−pass characteristics[13].

The solution of Eq. (24) is mainly Ricaati equation method and linear matrix inequality (LMI) method. Because the regular constraints of LMI method is less, it is used to solve Eq. (24) to obtain *H*−infinite robust controller $K(s)$ satisfying the condition. By repeatedly debugging the simulation software Matlab and observing the step response of system and the output of the controller, the final selection of the weighting function is

$$W_1(s) = \frac{0.5s + 0.99}{s + 0.029\,7} \tag{25}$$

$$W_2(s) = 4.30 \tag{26}$$

$$W_3(s) = \frac{s + 0.495}{0.03s + 0.99} \tag{27}$$

By multiple iterations, the *H*−infinite robust controller can be obtained as

$$K(s) = \frac{483.48s^3 + 418.52s^2 + 13.21s + 0.15}{s^4 + 1\,479s^3 + 6\,126s^2 + 11\,849s + 347} \tag{28}$$

Meanwhile the γ value is obtained as 1.561, and the controller is a 4−order controller.

5 Simulation and experiments

5.1 Numerical simulation

Initially, the open−loop transfer function obtained by Eq. (23) is applied as the nominal model, and the numerical simulation is carried out in Simulink. The step responses of the *H*−infinite robust controller, the conventional PID controller and the fuzzy controller are compared as shown in Fig. 14. From Fig. 14, it can be seen that the *H*−infinite robust controller has a shorter response time and almost no overshoot compared with the conventional PID controller and the fuzzy controller.

During the derivation of the open−loop transfer function in Eq. (23), considering that the rotational inertia I_z around the *z* axis of the abdominal operating ROV is calculated by Solidworks software, and assuming that there is a certain deviation from the actual value, and meanwhile, during the operation, the change in the displacement of the electric−driven push rod of the operating mechanism will also cause the variation of I_z, I_z is increased by 20%. At this moment, the transfer function of the controlled object will change, and with an unchanged controller, the comparison of step response when model changes is shown in Fig. 15. Comparing Fig. 14 and Fig. 15, it can be seen that the response time of the *H*−infinite robust controller increases after the rise of rotational inertia by 20%, but its overshoot is still significantly

smaller than that of the PID controller, and the response time is obviously better than that of the fuzzy controller.

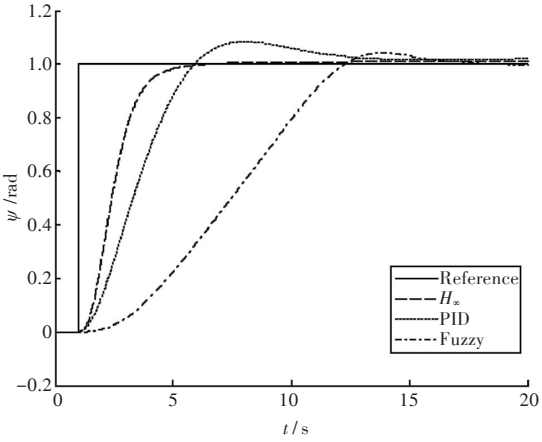

Fig.14 Comparison of the step response in nominal model

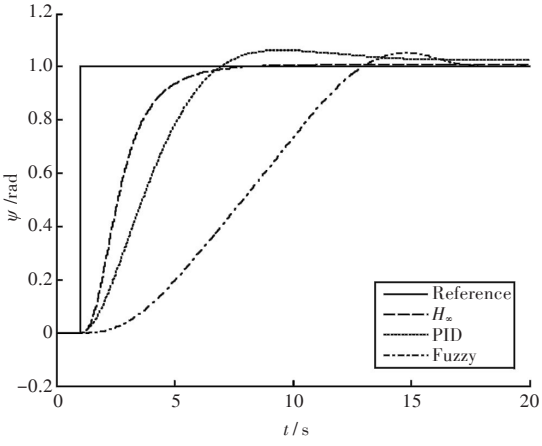

Fig.15 Comparison of the step response when I_z increase 20%

On the basis of the increase of the rotational inertia I_z by 20%, and considering that there is a certain deviation of motor time constant with the change of underwater environment, the time constant T is reduced by 20%, that is $T = 0.96$. When the controlled object model changes again, the comparison of step response is shown in Fig. 16 when the controller is unchanged.

Finally, taking the future second-phase project into account, if the funds are sufficient, there is possibility of conducting tests in the marine environment for abdominal operating ROV. The environmental disturbance can be added into the simulation of control system, that is the ocean current disturbance can be added to the conditions in Fig. 16, so as to test the robustness of controller under the current interference. Without loss of generality, the relative flow rate of the ocean current to ROV is assumed to be 1 kn, and the comparison of step responses is shown in Fig. 17.

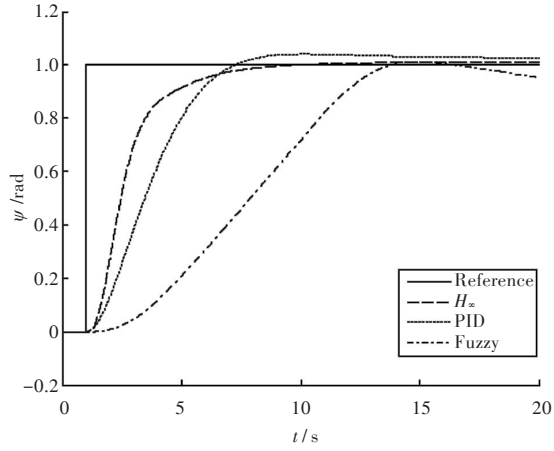

Fig.16 Comparison of the step response when I_z increase 20% and T decrease 20%

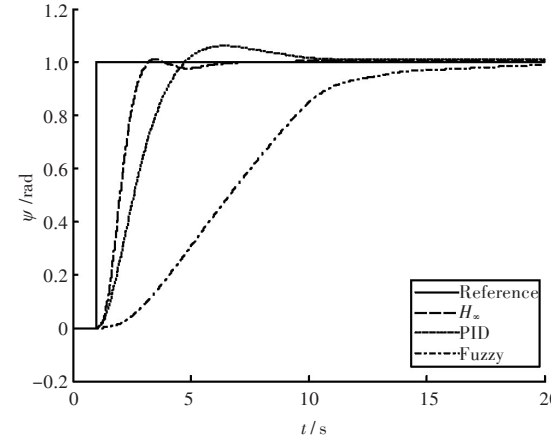

Fig.17 Comparison of the step response when I_z increase 20% and T decrease 20% and the current is 1 kn

Comparing Fig. 14–Fig. 16, it can be seen that the step response effect of H–infinite robust controller is always better than that of conventional PID controller and fuzzy controller in the case of some parameters perturbation existing in the orientation control model of abdominal operating ROV, and there is no obvious overshoot and oscillation, but showing strong robustness. After the addition of ocean current disturbance, the step response of the H–infinite robust controller is slightly overshot and oscillated, however, its comprehensive performance is still superior to that of the PID controller and the fuzzy controller.

5.2 Debug and test

1) Individual test on communication. Because the control system has to complete the RS485 serial communication with attitude and heading apparatus, surface monitoring computer, the driver board of main propeller and the driver board of side propeller in a control cycle, the appropriate control cycle and baud rate of communication require to be set by tests. The initial control cycle is 200 ms, and except that the

baud rate of the attitude instrument is 19 200 bit/s, baud rates of other three are all 9 600 bit/s. In order to improve the real-time capability of control system and shorten the control cycle, the baud rates of the surface monitoring computer, the driver board of main propeller, the driver board of side propeller and the PC104 embedded industrial computer are changed into 38 400 bit/s, while the baud rate of the attitude instrument remains unchanged, but the refreshing cycle of valid data is changed to 100 ms. Then the control cycle is shortened to 100 ms, which is decreased from the initial cycle by 50%, as shown in Table 2.

Table 2 The communication cycle and baud rate

Communication cycle/ms	Attitude and heading apparatus/ (bit·s^{-1})	The driver board of main and side propellers/ (bit·s^{-1})	Surface monitoring computer/ (bit·s^{-1})
200	19 200	9 600	9 600
100	19 200	38 400	38 400

2) System joint test. This test is mainly conducted in the laboratory environment by integrating the abdominal operating ROV equipment for the joint debugging. After testing, the control system can be operated stably.

3) Tank test on docking and recovery task. Due to the progress of the project, the current tank tests are mainly focused on the UUV search, docking and recovery test in the remote control mode, with certain automatic depth setting/orientation tests. With the experience of multiple tank experiments, the current operators can successfully complete the UUV search, docking and recovery tasks (Figs. 18-19) by observing the video-displaying interface of the surface monitoring software with the test records are shown in Table 3. Constrained by the test conditions, the maximum water flow rate of only 1 kn is simulated. Because the abdominal operating ROV has good horizontal-plane motion ability, even if the deviation of initial fore angle is large, the success rate of docking and recovery can still reach up to 90%, which meets the requirement of the project.

Fig.18 The ROV and UUV in docking

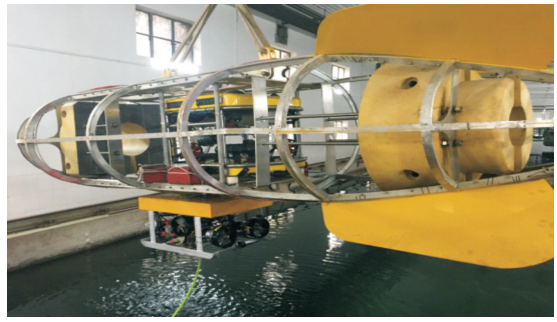

Fig.19 Lift the ROV and UUV after the docking

Table 3 The records of docking and recovery

Simulated flow rate/kn	Initial fore angle/ (°)	Number of tests	Number of success	Success rate/%
0	30	10	10	100
0	60	10	10	100
0	90	10	9	90
1	30	10	10	100
1	60	10	8	80
1	90	10	9	90

4) Automatic orientation test. Currently, it is mainly the manual recovery test in the whole process, and the operator's proficiency is improved through continuous exploration. Meantime, a small amount of automatic orientation control tests are supplemented to lay the foundation for the independent docking and recovery operation that is based on the visual in the second-phase of the renovation project. From the automatic orientation test results of abdominal operating ROV with initial fore angle set as 90° (see in Fig. 20), it can be seen that nearly no overshoot of the fore angle during the automatic orientation test but only slight chattering, and there is overall smooth rising with satisfying control performance.

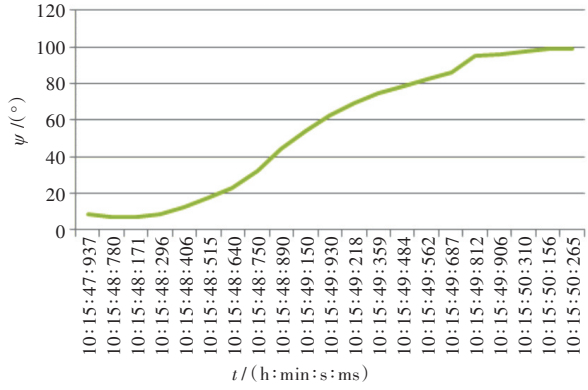

Fig.20 Result of the automatic orientation test

6 Conclusion

The systematic configuration and operating characteristics of a new abdominal operating ROV are introduced in this paper, and detailed description is con-

ducted aiming the hardware and software architecture of the control system. Based on the simplification of the six-DoF space motion equation of the underwater vehicle, the transfer function of automatic orientation control on horizontal plane is obtained, and an H-infinite robust automatic orientation controller based on the hybrid sensitivity is designed. The simulation results show that compared with the traditional PID controller, the proposed H-infinite robust automatic orientation controller has better static and dynamic performance, and its robustness is satisfying in the presence of some perturbation of the parameters. The design of hardware and software and control algorithms proposed in this paper are of reference significance for the other control systems of mobile robots, drones and bio-robots. At present, the abdominal operating ROV has completed the development, docking and recovery tasks of various functions and certain automatic control tests, and in the second-phase of the project, the independent operation based on the visual and other test topics will be studied.

References

[1] XU P F, MA L B, WANG L. Development and application of "SeaKite-Ⅱ" autonomous and remotely-operated vehicle [J]. China Science and Technology Achievements, 2012(20): 36-39(in Chinese).

[2] WANG Y, XU P F, HU Z. Motion control of "Seakite-Ⅱ" autonomous and remotely-operated vehicle [J]. Ship Electronic Engineering, 2014, 34(3): 56-60(in Chinese).

[3] ZHANG Y Y. The concept and technology development of autonomous underwater vehicle technology-taking "Bluefin-21" as an example[J]. China Terminology, 2014(Supp 1): 131-133(in Chinese).

[4] PYLE D, GRANGER R, GEOGHEGAN B, et al. Leveraging a large UUV platform with a docking station to enable forward basing and persistence for light weight AUVs [C]//Proceedings of 2012 Oceans. Hampton Roads, VA: IEEE, 2012: 1-8.

[5] HARDY T, BARLOW G. Unmanned Underwater Vehicle (UUV) deployment and retrieval considerations for submarines[C]//International Naval Engineering Conference and Exhibition 2008. Hamburg, Germany: INEC, 2008.

[6] RENILSON M. A simplified concept for recovering a UUV to a submarine [J]. Underwater Technology, 2014, 32(3): 193-197.

[7] DAI X F, BIAN X Q, SHI X C. Control for mating operation of multi-arm underwater vehicle[J]. Journal of Harbin Engineering University, 2001, 22(6): 9-11 (in Chinese).

[8] YU K Y, XU F A, WANG D T, et al. Design and application of the underwater recovering system for the untethered underwater vehicle "Explorer"[J]. Robot, 1996, 18(3): 179-184(in Chinese).

[9] LI X Y, LIU W D, YUE L N. Application of PC104 and VxWorks in deep-sea ROV control system[C]// Acoustics Academic Exchange Conference of Western China. Dunhuang: Acoustics Society of Sichuan Province, 2013(in Chinese).

[10] YANG X P. Control technology research of autonomous and remotely-operated vehicle [D]. Beijing: China Ship Research and Development Academy, 2012(in Chinese).

[11] WANG Y X. Research on the control system structure and heading control technique of "Hello I" ROV[D]. Hangzhou: Zhejiang University, 2012(in Chinese).

[12] ZHAI Y Y. Structure and control of subminiature underwater robot[D]. Shanghai: Shanghai University, 2007(in Chinese).

[13] ZHAO H, JIANG H Z, HAI J W, et al. Application of H_∞ mixed sensitivity control in hydraulic servo system [J]. China Mechanical Engineering, 2012, 13(3): 195-197(in Chinese).

腹部作业型水下机器人控制系统研制

张玮康[1], 王冠学[1], 徐国华[1], 刘畅[1], 申雄[2]

1 华中科技大学 船舶与海洋工程学院,湖北 武汉 430074

2 武汉第二船舶设计研究所,湖北 武汉 430205

摘　要:[**目的**]针对无人水下机器人(UUV)的回收任务要求,研制开发一台新式腹部作业型水下遥控机器人(ROV)。腹部作业型ROV不同于一般依赖机械手作业的传统ROV,其通过腹部作业机构完成与UUV的水下对接及回收。[**方法**]介绍腹部作业型ROV的系统组成及原理,提出一种以一体化工业加固计算机为水面监控单元,PC104嵌入式工业控制计算机为水下主控单元,各驱动板为驱动单元的控制系统架构。同时建立腹部作业型ROV的动力学模型,并设计水平面定向控制的H_∞鲁棒控制器。[**结果**]单项试验、系统联调及水池试验表明,腹部作业型ROV控制系统具有良好的实时性和可靠性,能够满足UUV回收任务的要求。[**结论**]该架构和算法对于其他移动机器人、无人机、仿生机器人的控制系统开发均具有参考意义。

关键词: 腹部作业型水下遥控机器人;控制系统;PC104;H_∞鲁棒控制